

CMS Physics Analysis Summary

Contact: cms-pag-conveners-exotica@cern.ch

2016/08/05

Search for heavy stable charged particles with 12.9 fb^{-1} of 2016 data

The CMS Collaboration

Abstract

Results from searches for heavy, stable, charged particles are presented using data from pp collisions at a center-of-mass energy of 13 TeV using 12.9 fb^{-1} data from 2016 LHC operations. The distinctive signatures of large dE/dx and long time-of-flight are used to discriminate signal from background using the CMS detector. The data are consistent with expected background. Upper limits are set on the cross section for production of long-lived gluinos, scalar tops, scalar taus, and lepton-like fermions. In addition, lower mass limits are set for these signals. The mass limit on gluinos is found to be 1850 GeV.

1 Introduction

Many extensions of the standard model (SM) include heavy, long-lived, charged particles that might have speed, v , significantly less than the speed of light, c , [1–3] and/or charge, Q , not equal to $\pm 1e$ [4–7]. Those with lifetimes greater than a few nanoseconds can travel distances larger than the typical collider detector and appear stable like pions or kaons. These particles can be generically referred to as heavy stable charged particles (HSCPs). Because particle identification algorithms at hadron collider experiments generally assume signatures characteristic of SM particles, e.g., speed close to the speed of light and a charge of $\pm 1e$, HSCPs may go unidentified. A further complication arises from the fact that HSCPs might be charged during only a part of their passage through detectors, further limiting the ability of standard algorithms to identify them. For these reasons, dedicated searches have been developed.

For HSCP masses greater than ~ 100 GeV, a significant fraction of particles produced at the CERN LHC will have velocity, $\beta \equiv v/c$, less than 0.9. It is possible to distinguish $|Q| \geq 1e$ particles with $\beta < 0.9$ from speed-of-light SM particles through their higher rate of energy loss via ionization (dE/dx) or through their longer time-of-flight (TOF) to the outer detectors. In the CMS detector, both dE/dx and TOF variables are used to search for HSCP particles in two analysis channels: "tracker-only" and "tracker+TOF" (see Section 4).

The dependence of dE/dx on particle momentum is described by the Bethe-Bloch formula [8]. In the momentum range of interest at the LHC (10–1000 GeV), SM particles have nearly uniform ionization energy loss (≈ 3 MeV/cm). Searching for candidates with larger dE/dx gives sensitivity to massive particles with $|Q| = 1e$ and particles with $|Q| > 1e$.

Previous collider searches for HSCPs have been performed at LEP [9–12], HERA [13], the Tevatron [14–17], and the LHC [18–31]. The results from these searches have placed significant bounds on beyond the SM theories [32, 33], such as lower limits at 95% confidence level on the mass of: gluinos, 1098 GeV; scalar top quarks, 737 GeV; and pair-produced scalar taus, 223 GeV.

Presented here are searches for singly and multiply charged HSCPs using 12.9 fb^{-1} of data collected with the CMS detector at $\sqrt{s} = 13$ TeV in 2016.

2 Signal Benchmarks

The HSCP searches employ several signal models to account for a range of signatures that are experimentally accessible.

The first type of signal consists of HSCPs that interact via the strong force and hadronize with SM quarks to form R -hadrons. As in Refs. [31, 34], events involving pair production of \tilde{g} and \tilde{t}_1 , with mass values in the range 300–2600 GeV, are generated under the Split SUSY scenarios. Gluinos are generated under the high squark mass (10 TeV) assumption. PYTHIA v8.153 [35], with the default tune CUETP8M1, is used to generate the 13 TeV Monte Carlo (MC) samples. The fraction, f , of produced \tilde{g} hadronizing into a \tilde{g} -gluon state (R -gluonball) is an unknown parameter of the hadronization model and affects the fraction of R -hadrons that are neutral at production. For this search, results are obtained for two different values of f , 0.1 and 0.5. Unless otherwise specified, the value $f = 0.1$ should be assumed. As in Refs. [31, 34], two scenarios of R -hadron strong interactions with matter are considered: the first follows the model in Refs. [36, 37] while the second is one of complete charge suppression, where any nuclear interaction leaves the R -hadron as a neutral particle. Both the tracker-only and tracker+TOF analyses are used to search for these signals, but the tracker-only analysis is expected to have

sensitivity even in the charge suppressed scenario.

The second type of signal consists of HSCPs that behave like leptons. The minimal gauge mediated supersymmetry breaking (mGMSB) model [38] is selected as a benchmark for lepton-like HSCPs. Production of supersymmetric quasi-stable leptons ($\tilde{\tau}_1$) at the LHC can proceed either directly or via production of heavier supersymmetric particles (mainly squarks and gluino pairs) that decay and lead to one or more $\tilde{\tau}_1$ particles at the end of the decay chain. This process is generally dominant because the direct production process is electroweak. The mGMSB model is explored using the SPS7 slope [39], which has the stau ($\tilde{\tau}$) as the next-to-lightest supersymmetric particle (NLSP). The particle mass spectrum and the decay table are produced with the program ISASUGRA [40] version 7.69. The mGMSB parameter Λ is varied from 31 to 160 TeV, with fixed parameters $N_{\text{mes}} = 3$, $\tan \beta = 10$, $\mu > 0$, $C_{\text{grav}} = 10000$, and $M_{\text{mes}}/\Lambda = 2$. The large value of C_{grav} results in a long-lived stau, while $\Lambda = 31\text{--}510$ TeV gives a stau mass of 100 to 1600 GeV. The produced SUSY mass spectrum is input into PYTHIA v6.4 [35] with Z2star tune as the generator for a MC simulation at 13 TeV. Two $\tilde{\tau}$ samples are generated for each SUSY point: one with all processes (labeled "GMSB stau") and one with only direct pair production (labeled "Pair Prod. stau"). The pair-produced stau includes only $\tilde{\tau}_1$, which is predominantly $\tilde{\tau}_R$ for these model parameters. The tracker-only and tracker+TOF analyses are both used to search for these signals.

The last type of signal is based on modified Drell–Yan production of long-lived lepton-like fermions. In this scenario, new massive spin-1/2 particles have arbitrary electric charge but are neutral under SU(3)C and SU(2)L, and therefore couple only to the photon and the Z boson. PYTHIA v6.4 [35] with Z2star tune is used to generate these 13 TeV MC signal samples. Simulations for lepton-like fermions are generated with masses ranging from 100 to 2600 GeV and for electric charges $|Q| = 1e$ and $2e$.

Different PYTHIA tunes used in generating the samples above were studied and the effects on kinematic distribution were negligible for the HSCPs considered. The tracker-only and tracker+TOF analyses are both expected to have sensitivity to $|Q| = 2e$ HSCPs.

In all signal samples, simulated minimum bias events are overlaid with the primary collision to produce the effect of additional interactions in the same beam crossing (pileup).

3 CMS Detector

The central feature of the CMS apparatus is a superconducting solenoid of 6 m internal diameter. Within the superconducting solenoid volume are a silicon tracker, a lead tungstate crystal electromagnetic calorimeter, and a brass and scintillator hadron calorimeter, each composed of a barrel and two endcap sections. Outside the solenoid, forward calorimeters extend the pseudorapidity [41] coverage provided by the barrel and endcap detectors. Muons are measured in gas-ionization detectors embedded in the steel flux-return yoke outside of the solenoid. The missing transverse momentum vector \vec{p}_T^{miss} is defined as the projection on the plane perpendicular to the beam axis of the negative vector sum of the momenta of all reconstructed particles in an event. Its magnitude is referred to as E_T^{miss} .

The silicon tracker measures charged particles within the pseudorapidity range $|\eta| < 2.5$. It consists of 1440 silicon pixel and 15 148 silicon strip detector modules and is located in the 3.8 T field of the superconducting solenoid. Isolated particles of $p_T = 100$ GeV and with $|\eta| < 1.4$ have track resolutions of 2.8% in p_T and 10 (30) μm in the transverse (longitudinal) impact parameter [42]. Muons are measured in the pseudorapidity range $|\eta| < 2.4$, with planes made

using three technologies: drift tubes (DTs), cathode strip chambers (CSCs), and resistive plate chambers (RPCs). Matching muons to tracks measured in the silicon tracker results in a relative transverse momentum resolution for muons with $20 < p_T < 100$ GeV of 1.3–2.0% in the barrel and better than 6% in the endcaps. The p_T resolution in the barrel is better than 10% for muons with p_T up to 1 TeV [43]. The first level (L1) of the CMS trigger system, composed of custom hardware processors, uses information from the calorimeters and muon detectors to select events of interest within a fixed time interval of less than 4 μ s. The high-level trigger (HLT) processor farm further decreases the event rate from around 100 kHz to less than 1 kHz, before data storage. A more detailed description of the CMS detector, together with a definition of the coordinate system used and the relevant kinematic variables, can be found in Ref. [41].

3.1 dE/dx Measurements

As in Ref. [28], a dE/dx discriminator, I_{as} is used to distinguish SM particles from HSCP candidates. The discriminator is given by:

$$I_{as} = \frac{3}{N} \times \left(\frac{1}{12N} + \sum_{i=1}^N \left[P_i \times \left(P_i - \frac{2i-1}{2N} \right)^2 \right] \right), \quad (1)$$

where N is the number of measurements in the silicon-tracker detectors, P_i is the probability for a minimum-ionizing particle to produce a charge smaller or equal to that of the i -th measurement for the observed path length in the detector, and the sum is over the track measurements ordered in terms of increasing P_i .

In addition, the dE/dx of a track is estimated using a harmonic-2 estimator:

$$I_h = \left(\frac{1}{N_{85\%}} \sum_i^{N_{85\%}} c_i^{-2} \right)^{-1/2}, \quad (2)$$

where c_i is the charge per unit path length in the sensitive part of the silicon detector of the i -th track measurement. The harmonic-2 estimator has units MeV/cm and the summation is over the 85% pixel and strip silicon detector measurements with the highest charge. Ignoring the 15% measurements with the lowest charge increases the resilience of the estimator against instrumental biases. This procedure is not necessary for I_{as} which is, by construction, robust against that type of bias.

The mass of a candidate particle can be calculated [34], from its momentum and I_h dE/dx estimate, based on the relationship :

$$I_h = K \frac{m^2}{p^2} + C, \quad (3)$$

where the empirical parameters K and C are determined from data using a sample of low-momentum protons. For 2016 data, the values of K and C were determined to be 2.6 ± 0.2 and 3.9 ± 0.4 , respectively. As the momentum reconstruction is done assuming $|Q| = 1e$ particles, the relation above would lead to an accurate mass reconstruction only for singly charged particles.

The HSCP candidates are primarily selected using the I_{as} discriminator (see Section 5) because it has a better signal-to-background discriminating power in comparison to the I_h estimator or the mass. Nonetheless, the mass is used at the last stage of the analysis, after the I_{as} selection, to further discriminate between signal and backgrounds since the latter tend to have a low reconstructed mass.

3.2 Time-of-flight Measurements

The time-of-flight to the muon system can be used to discriminate between particles traveling at near the speed of light and slower candidates. Both the DT and the CSC muon systems measure the time of each hit. For the CSC this feature was designed mainly for the purpose of proper bunch crossing reconstruction. In the DTs the time measurement is used to make a precision position measurement. The synchronization works in a such a way that a relativistic muon produced at the interaction point gives an aligned pattern of hits in consecutive DT layers. For a slower HSCP particle, hits in each DT layer will be reconstructed as shifted with respect to its true position and will form a zigzag pattern with an offset proportional to the particle delay, δ_t . In the CSC such delay is measured directly via sampling. Each δ_t measurement can be used to determine the track β^{-1} via the equation:

$$\beta^{-1} = 1 + \frac{c\delta_t}{L} \quad (4)$$

where L is the flight distance. The track β^{-1} value is calculated as the weighted average of the β^{-1} measurements from the DT and CSC systems associated with the track. The weight for the i^{th} DT measurement is given by:

$$w_i = \frac{(n-2)}{n} \frac{L_i^2}{\sigma_{DT}^2} \quad (5)$$

where n is the number of ϕ projection measurements found in the muon chamber producing the measurement and σ_{DT} is the time resolution of the DT measurements, for which the measured value of 3 ns is used. The factor $(n-2)/n$ accounts for the fact that residuals are computed using the two parameters of a straight line determined from the same n measurements (minimal number of hits in a given DT chamber that allows for at least one residual calculation is $n = 3$). The weight for the i^{th} CSC measurement is given by:

$$w_i = \frac{L_i^2}{\sigma_i^2} \quad (6)$$

where σ_i , the measured time resolution, is 7.0 ns for cathode strip measurements and 8.6 ns for anode wire measurements.

The resolution on the weighted average β^{-1} measurement is approximately 0.065 in both the DT and CSC subsystems.

4 Data Selection

HSCPs are searched for in two ways: (1) requiring tracks to be reconstructed in both the silicon detectors and the muon system, referred to as the tracker+TOF analysis; (2) only requiring tracks be reconstructed in the silicon detectors, the tracker-only analysis.

All events pass a trigger requiring either the reconstruction of a muon with high transverse momentum or the calculation of large E_T^{miss} , which is defined by a negative sum over transverse momenta of all final-state particles in the event, using an online particle-flow algorithm [44].

The muon trigger is more efficient than the E_T^{miss} trigger for all HSCP models with the exception of the charged suppressed R -hadron model, but it is not efficient for particles that are too slow ($\beta < 0.6$).

The E_T^{miss} trigger can recover some events in which the HSCP is charged in the tracker and neutral in the muon subsystem. The particle-flow algorithm rejects tracks reconstructed only

in the tracker with a track p_T much greater than the matched energy deposited in the calorimeter [45], as would be the case for HSCPs that become neutral in the calorimeter. Thus the E_T^{miss} calculation will only include the energy these HSCPs deposit in the calorimeter, roughly 10–20 GeV. Significant E_T^{miss} can result in events where one or more HSCPs fail to be reconstructed as muon candidates.

For both analyses, the muon trigger requires $p_T > 50$ GeV and the E_T^{miss} trigger requires $E_T^{\text{miss}} > 170$ GeV. Using multiple triggers for both analyses allows for increased sensitivity to HSCP candidates that arrive in the muon system very late, as well as for hadron-like HSCPs, which are sometimes charged only in the tracker.

For the tracker-only analysis, all events are required to have a candidate track with $p_T > 55$ GeV (as measured in the tracker), relative uncertainty on p_T (σ_{p_T}/p_T) less than 0.25, $|\eta| < 2.1$, track fit $\chi^2/\text{dof} < 5$, and magnitudes of the impact parameters d_z and d_{xy} both less than 0.5 cm (d_z and d_{xy} are the longitudinal and transverse impact parameters with respect to the vertex with the minimal d_z). The cuts on the impact parameters are very loose compared to the resolution for tracks in the tracker. Candidates must pass isolation requirements in the tracker and calorimeter. The tracker isolation criteria is $\sum p_T < 50$ GeV, where the sum is over all tracks (except the candidate) within $\Delta R = \sqrt{(\Delta\eta)^2 + (\Delta\phi)^2} < 0.3$. The calorimeter isolation criteria is $E/p < 0.3$, where E is the sum of energy deposited in the calorimeter towers within $\Delta R < 0.3$ and p is the track momentum reconstructed from the tracker. Candidates must have at least two measurements in the silicon pixel detector and at least six measurements in the strip detectors. In addition, there must be measurements in at least 80% of the silicon layers between the first and last measurements of the track. To reduce the rate of contamination from clusters with large energy deposition due to overlapping tracks, a cleaning procedure is applied to remove clusters in the silicon strip tracker that are not consistent with the passage of a single charged particle (e.g., a narrow cluster with most of the energy deposited in one or two strips). After cluster cleaning, there must be at least six measurements in the silicon tracker that are used for the dE/dx calculation.

The tracker+TOF analysis applies the same criteria, but additionally requires a reconstructed muon matched to the track in the inner detectors. At least eight independent time measurements are required for the TOF computation. Finally, $1/\beta > 1$ and $\sigma_{1/\beta} < 0.15$ are required.

5 Background Prediction

For both analyses, results are based upon a comparison of the number of candidates passing the selection criteria defining the signal region (see Section 7) with the number of predicted background events in that region. Candidates passing the preselection criteria (Section 4) are subject to two (or three) additional criteria to improve the signal-to-background discrimination. By choosing two uncorrelated criteria it is possible to predict the background using the *ABCD* method. In this approach, the expected background in the signal region, D , is estimated by BC/A , where B and C are the number of candidates that fail the first and second criterion, respectively, while A is the number of candidates that fail both criteria.

For the tracker-only analysis, the two criteria are $p_T > 65$ GeV and $I_{as} > 0.3$. The candidates passing only the I_{as} requirement fall into the B region and those passing only the p_T requirement fall into the C region. The B and C candidates are then used to form a binned probability density function in I_h and p , respectively, such that, using the mass value (Eq. (3)), the full mass spectrum of the background in the signal region D can be predicted. However, the η distribution of candidates at low dE/dx differs from the distribution of the candidates at high dE/dx .

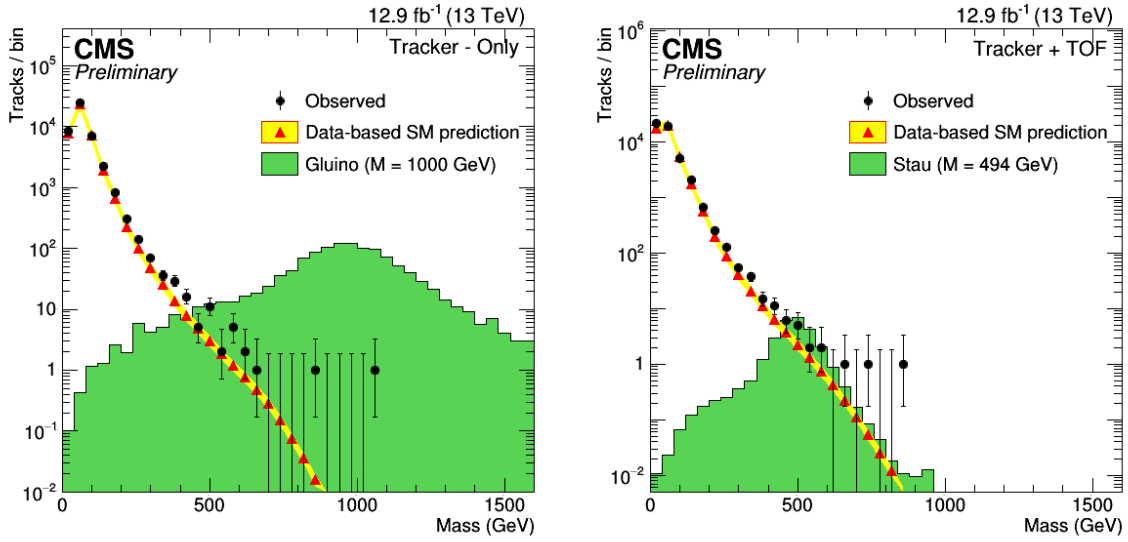


Figure 1: Observed and predicted mass spectra for candidates entering the tracker-only (left) and tracker+TOF (right) signal region for the loose selection. The expected distribution for a representative signal is shown in green.

To correct for this, events in the C region are weighted such that the η distribution matches that in the B region.

For the tracker+TOF analysis, three criteria are used, $p_T > 65 \text{ GeV}$, $I_{as} > 0.175$, and $1/\beta > 1.250$, creating eight regions labeled $A - H$. Region D represents the signal region, with events passing all three criteria. The candidates in the A , F , and G regions pass only the $1/\beta$, I_{as} , and p_T criteria, respectively, while the candidates in the B , C , and H regions fail only the p_T , I_{as} , and $1/\beta$ criteria, respectively. The E region contains events that fail all three criteria. Background estimates can be made from several different combinations of these regions. The combination $D = AGF/E^2$ is used because it yields the smallest statistical uncertainty. As in the tracker-only analysis, events in the G region are reweighted to match the η distribution in the F region. The spread in background estimates from the other combinations is less than 20%, which is taken as the systematic uncertainty in the background estimate. The same 20% systematic uncertainty is used for the tracker-only analysis.

Samples with a loose selection (dominated by background tracks) are used to test the background prediction. The loose selection sample for the tracker-only analysis is defined as $p_T > 60 \text{ GeV}$ and $I_{as} > 0.10$. The loose selection sample for the tracker+TOF analysis is defined as $p_T > 60 \text{ GeV}$, $I_{as} > 0.05$, and $1/\beta > 1.05$. Figure 1 shows the observed and predicted mass spectra for these samples.

For each analysis, fixed selections on the appropriate set of I_{as} , p_T , and $1/\beta$ are used to define the final signal region (and the regions for the background prediction). These values are chosen to give the best discovery potential over the signal mass regions of interest. For both analyses, an additional requirement on the reconstructed mass is applied. The specific requirement is adapted to each HSCP model. For a given mass and model, the mass requirement is $M \geq M_{reco} - 2\sigma$ where M_{reco} is the average reconstructed mass for the given mass M_{HSCP} and σ is the expected resolution. Simulation is used to determine M_{reco} and σ .

Table 1 lists the final selection criteria, the predicted number of background events, and the number of events observed in the signal region. Agreement between prediction and obser-

Table 1: Selection criteria for the various subanalyses with the number of predicted and observed events.

	Selection cuts				Numbers of events 2016	
	p_T (GeV)	I_{as}	$1/\beta$	Mass (GeV)	Pred.	Obs.
Trk-only	> 65	> 0.3	-	> 0	92.4 ± 18.9	94
				> 100	43.2 ± 8.9	46
				> 200	4.3 ± 0.9	7
				> 300	0.86 ± 0.18	0
				> 400	0.25 ± 0.05	0
Trk+TOF	> 65	> 0.175	> 1.250	> 0	53.1 ± 10.6	50
				> 100	7.7 ± 1.5	8
				> 200	0.82 ± 0.17	2
				> 300	0.15 ± 0.03	1
				> 400	0.04 ± 0.01	1

vation is seen for both tracker-only and tracker+TOF analyses. Figure 2 shows the observed and predicted mass distribution for the tracker-only and tracker+TOF analyses with the final selection.

6 Systematic Uncertainties

The sources of systematic uncertainty considered are those related to the background prediction, the signal acceptance, and the integrated luminosity. The uncertainty on the integrated luminosity is 6.2% at $\sqrt{s} = 13$ TeV. The uncertainties on the background predictions are described in Section 5.

The signal acceptance is obtained from Monte Carlo samples of the various signals processed through the full detector simulation (Section 2). Systematic uncertainties are derived by comparing the response of the detector to the data and the MC samples. The relevant uncertainty sources are discussed below.

The signal trigger efficiency is dominated by the muon triggers for all the models except the charge-suppressed ones. The uncertainty on the muon trigger efficiency has many contributions. A correction is applied to the muon triggers for the MC to account for a larger difference between data and MC observed in 2016. For slow moving particles, the effect of timing synchronization of the muon system is tested by shifting the arrival times in MC by the synchronization accuracy observed in data, resulting in an efficiency change of less than 4% for most samples and up to 8% for the 2.4 TeV gluino sample. The uncertainty in the E_T^{miss} trigger efficiency is found by varying the jet energy scale in the simulation of the HLT as it is done in data. The E_T^{miss} uncertainty is found to be less than 12% for all samples. The total trigger uncertainty is found to be less than 13% for all the samples since the muon trigger inefficiencies are often compensated by the E_T^{miss} trigger and vice versa.

Low momentum protons are used to compare the observed and simulated distributions for the energy loss in the silicon tracker, I_h and I_{as} . The dE/dx distributions of signal samples are varied by the observed differences to estimate the systematic uncertainty. The uncertainty

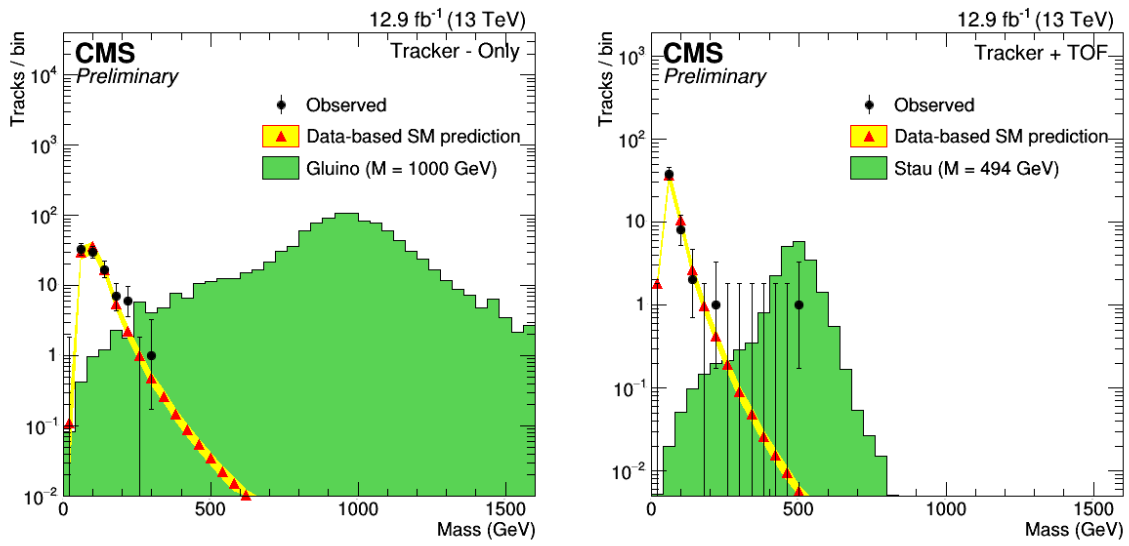


Figure 2: Observed and predicted mass spectra for candidates entering the tracker-only (left) or tracker+TOF (right) signal region for the final selection. The expected distribution for a representative signal is shown in green.

in the signal acceptance is at most 13(7)% for tracker-only(tracker+TOF). For the tracker-only analysis, it is below 10% for most of the signal samples.

A bias in the energy loss measurement due to highly ionizing particles (HIPs), such as low momentum protons produced in pp collisions earlier than the triggering collision, was considered as a source of uncertainty in the I_h estimate. In 2016, the LHC collision rate increased, causing an increase of the HIP rate compared to previous runs. The effects of HIP particles were applied to the simulation with a rate corresponding to the level observed in the 2016 data sample. The uncertainty on this rate is found to be 25% and 80% for pixel and strip sensors respectively. Varying the HIP rate in the simulation by these amounts leads to a change in signal efficiency of at most 8% for both analyses.

Dimuon events are used to test the MC simulation of $1/\beta$ through comparison to data. An offset of at most 1.5% is found for the muon system. The resulting uncertainty in the signal acceptance is found to be less than 5% by shifting $1/\beta$ by this amount.

As in Ref. [30], the uncertainties on the efficiencies for muon reconstruction [43] and track reconstruction [46] are less than 2% each. The track momentum uncertainty is estimated by shifting the momentum from the inner track as in Ref. [30]. This uncertainty is found to be less than 5% for most of the samples, increasing to 13% for masses above 2 TeV.

The uncertainty in the number of pileup events is evaluated using a 5% variation in the minimum bias cross section used to calculate the weights applied to signal events in order to reproduce the pileup observed in data. This results in uncertainties due to pileup of less than 1%.

The total systematic uncertainty in the signal efficiency is the sum in quadrature of the uncertainties due to the sources discussed above. For all the samples, it is less than 20% for both analyses.

Table 2 summarizes the systematic uncertainties for the two analyses. As the uncertainty often depends on the model and HSCP mass, the largest systematic uncertainty is reported for each

Table 2: Systematic uncertainties for the various HSCP searches. All values are relative uncertainties. The middle columns show the range of values while the last two columns show two example cases: gluino ($f=0.1$, $M=1800$ GeV) and GMSB stau ($M=651$ GeV).

Source of Systematic Uncertainties	Relative Uncertainty (%)		Gluino $M=1800$ GeV	Stau $M=651$ GeV
Signal acceptance	Trk-only	Trk+TOF	Trk-only	Trk+TOF
- Trigger efficiency	13	13	13	13
- Track momentum scale	0 – 5	0 – 14	0.8	0.7
- Track reconstruction	0 – 2	0 – 2	0.5	0.7
- Ionization energy loss	0 – 13	0 – 7	3	3
- HIP background effect	0 – 10	0 – 10	7	10
- Time-of-flight	-	0 – 6	–	2
- Muon reconstruction	-	2	–	2
- Pileup	0 – 2	0 – 2	0.4	0.2
Total uncertainty on signal acceptance	0 – 20	0 – 20	15	17
Collision background uncertainty	20	20	20	20
Luminosity uncertainty	6.2		6.2	

source.

7 Results

There is good agreement between the predicted background and the observed number of events. One event with mass 510 ± 160 GeV is found in the tracker+TOF analysis. Cross section limits are placed at 95% confidence level (CL) using a CL_s approach [47, 48] where p-values are computed with a profile likelihood technique [49] that uses a lognormal model [50, 51] for the nuisance parameters. These are the integrated luminosity, the signal acceptance, and the expected background in the signal region.

The observed limits are shown in Fig. 3 for both tracker-only and tracker+TOF analyses along with the theoretical predictions. For the gluino and stop pair production, the theoretical cross sections are computed at NLO+NLL [52–55] using PROSPINO [56] with CTEQ6.6M PDFs [57]. The uncertainty bands on the theoretical cross sections include the PDF uncertainty as well as the μ and α_s scale uncertainties. Mass limits are obtained from the intersection of the observed limit and the central value of the theoretical cross section.

From the final results, 95% CL limits on the production cross section are shown in Tables 3, 4, 5, and 6 for gluino, stop, stau, and modified Drell–Yan signals, respectively. The limits are determined from the numbers of events passing all final criteria (including the mass criteria). Figure 3 shows the limits as a function of mass for the tracker-only and tracker+TOF analyses. The tracker-only analysis excludes $f = 0.1$ gluino masses below 1850 and 1840 GeV for the cloud interaction model and charge suppressed model, respectively. Stop masses below 1250(1220) GeV are excluded for the cloud (charge suppressed) models. In addition, the tracker+TOF analysis excludes $\tilde{\tau}_1$ masses below 660(360) GeV for the GMSB (pair production) model. Drell–Yan signals with $|Q| = 1e$ and $2e$ are excluded below 730 and 890 GeV, respectively.

Table 3: Summary of the p_T , I_{as} , $1/\beta$, and mass thresholds, the observed and predicted yields passing these criteria, and the resulting expected (Exp.) and observed (Obs.) cross section limits for gluino signals. The signal efficiency and theoretical (Th.) cross section are also listed.

Mass	Requirements				Yields		Signal Eff.	σ (pb)		
	p_T (GeV)	I_{as}	$1/\beta$	M (GeV)	Predicted	Data		Th.	Exp.	Obs.
Gluino ($f = 0.1$) particles with the tracker-only analysis										
400	65	0.300	/	80	62 ± 13	61	0.150	9.5E+01	1.4E-02	1.3E-02
800	65	0.300	/	330	0.57 ± 0.12	0	0.202	1.5E+00	1.1E-03	1.1E-03
1200	65	0.300	/	520	0.072 ± 0.015	0	0.196	8.4E-02	1.2E-03	1.2E-03
1600	65	0.300	/	590	0.037 ± 0.008	0	0.148	8.0E-03	1.6E-03	1.6E-03
2000	65	0.300	/	590	0.037 ± 0.008	0	0.102	9.7E-04	2.3E-03	2.3E-03
2400	65	0.300	/	640	0.024 ± 0.005	0	0.069	1.3E-04	3.5E-03	3.5E-03
Gluino charged suppressed ($f = 0.1$) particles with the tracker-only analysis										
400	65	0.300	/	120	26.8 ± 5.6	31	0.087	9.5E+01	1.4E-02	1.7E-02
600	65	0.300	/	240	2.15 ± 0.44	1	0.132	9.1E+00	2.9E-03	2.3E-03
1200	65	0.300	/	510	0.079 ± 0.016	0	0.176	8.4E-02	1.3E-03	1.3E-03
1600	65	0.300	/	560	0.049 ± 0.010	0	0.139	8.0E-03	1.7E-03	1.7E-03
2000	65	0.300	/	550	0.054 ± 0.011	0	0.094	9.7E-04	2.6E-03	2.6E-03
2400	65	0.300	/	520	0.072 ± 0.015	0	0.057	1.3E-04	4.2E-03	4.2E-03
Gluino ($f = 0.5$) particles with the tracker-only analysis										
400	65	0.300	/	70	72 ± 15	72	0.084	9.5E+01	2.8E-02	2.8E-02
800	65	0.300	/	330	0.57 ± 0.12	0	0.117	1.5E+00	2.0E-03	2.0E-03
1200	65	0.300	/	510	0.079 ± 0.016	0	0.113	8.4E-02	2.3E-03	2.3E-03
1600	65	0.300	/	590	0.037 ± 0.008	0	0.085	8.0E-03	2.9E-03	2.9E-03
2000	65	0.300	/	580	0.041 ± 0.008	0	0.056	9.7E-04	4.3E-03	4.3E-03
2400	65	0.300	/	650	0.022 ± 0.004	0	0.038	1.3E-04	6.4E-03	6.4E-03

The mass limits obtained at $\sqrt{s} = 13$ TeV for various HSCP signal models are summarized in Table 7. An increase in the mass limit is obtained for all models with a significant QCD production cross section (gluinos, stops, and inclusive production of staus), thanks to the higher center-of-mass energy pp collisions delivered by the LHC.

8 Summary

A number of searches for heavy stable charged particles produced in proton-proton collisions at $\sqrt{s} = 13$ TeV using the CMS detector are presented. Two complementary analyses were performed: a search using only the tracker and a search using both the tracker and the muon system. Data are found to be compatible with the background expectation. Mass limits for gluinos, stops, staus, and multiply charged particles are calculated. The models for R -hadron-like HSCPs include varying the fraction of \tilde{g} -gluon production and two different interaction models producing a variety of exotic experimental signatures. The limits, ranging up to 1850 GeV for gluinos, represent significant improvements on previous limits from the LHC.

References

- [1] M. Drees and X. Tata, “Signals for heavy exotics at hadron colliders and supercolliders”, *Phys. Lett. B* **252** (1990) 695, doi:10.1016/0370-2693(90)90508-4.
- [2] M. Fairbairn et al., “Stable massive particles at colliders”, *Phys. Rept.* **438** (2007) 1, doi:10.1016/j.physrep.2006.10.002, arXiv:hep-ph/0611040.

Table 4: Summary of the p_T , I_{as} , $1/\beta$, and mass thresholds, the observed and predicted yields passing these criteria, and the resulting expected (Exp.) and observed (Obs.) cross section limits for stop signals. The signal efficiency and theoretical (Th.) cross section are also listed.

Mass	Requirements				Yields		Signal Eff.	σ (pb)		
	p_T (GeV)	I_{as}	$1/\beta$	M (GeV)	Predicted	Data		Th.	Exp.	Obs.
Stop particles with the tracker-only analysis										
200	65	0.300	/	0	92 ± 19	94	0.176	6.1E+01	1.6E-02	1.6E-02
600	65	0.300	/	90	53 ± 11	53	0.241	1.7E-01	7.7E-03	7.6E-03
1000	65	0.300	/	300	0.86 ± 0.18	0	0.232	6.0E-03	1.5E-03	1.0E-03
1400	65	0.300	/	470	0.117 ± 0.024	0	0.199	4.5E-04	1.2E-03	1.2E-03
1800	65	0.300	/	520	0.072 ± 0.015	0	0.149	4.6E-05	1.6E-03	1.6E-03
2200	65	0.300	/	530	0.065 ± 0.013	0	0.098	6.0E-06	2.5E-03	2.5E-03
2600	65	0.300	/	490	0.096 ± 0.020	0	0.064	1.0E-06	3.7E-03	3.7E-03
Stop charged suppressed particles with the tracker-only analysis										
200	65	0.300	/	0	92 ± 19	94	0.046	6.1E+01	6.0E-02	6.3E-02
600	65	0.300	/	80	62 ± 13	61	0.162	1.7E-01	1.3E-02	1.2E-02
1000	65	0.300	/	280	1.14 ± 0.24	1	0.188	6.0E-03	1.7E-03	1.7E-03
1800	65	0.300	/	450	0.144 ± 0.030	0	0.124	4.6E-05	1.9E-03	1.9E-03
2200	65	0.300	/	450	0.144 ± 0.030	0	0.084	6.0E-06	2.9E-03	2.9E-03
2600	65	0.300	/	380	0.311 ± 0.064	0	0.054	1.0E-06	4.4E-03	4.4E-03

Table 5: Summary of the p_T , I_{as} , $1/\beta$, and mass thresholds, the observed and predicted yields passing these criteria, and the resulting expected (Exp.) and observed (Obs.) cross section limits for stau signals. The signal efficiency and theoretical (Th.) cross section are also listed.

Mass	Requirements				Yields		Signal Eff.	σ (pb)		
	p_T (GeV)	I_{as}	$1/\beta$	M (GeV)	Predicted	Data		Th.	Exp.	Obs.
Inclusive prod. of stau particles with the tracker+TOF analysis										
200	65	0.175	1.250	10	2.63 ± 0.53	5	0.276	2.8E-01	1.4E-03	2.3E-03
308	65	0.175	1.250	120	0.163 ± 0.033	0	0.429	2.5E-02	5.5E-04	5.5E-04
494	65	0.175	1.250	260	0.008 ± 0.002	0	0.569	1.9E-03	4.2E-04	4.2E-04
651	65	0.175	1.250	360	0.002 ± 0.000	0	0.628	4.1E-04	3.8E-04	3.8E-04
1029	65	0.175	1.250	540	0.000 ± 0.000	0	0.665	2.2E-05	3.6E-04	3.6E-04
1599	65	0.175	1.250	810	0.000 ± 0.000	0	0.481	1.0E-06	5.1E-04	5.1E-04
Pair prod. of stau particles with the tracker+TOF analysis										
200	65	0.175	1.250	50	2.05 ± 0.41	2	0.235	8.0E-03	1.6E-03	1.6E-03
308	65	0.175	1.250	120	0.163 ± 0.033	0	0.294	1.5E-03	8.1E-04	8.1E-04
494	65	0.175	1.250	250	0.010 ± 0.002	0	0.387	1.9E-04	6.2E-04	6.2E-04
651	65	0.175	1.250	340	0.002 ± 0.001	0	0.450	4.9E-05	5.4E-04	5.4E-04
1029	65	0.175	1.250	560	0.000 ± 0.000	0	0.497	4.0E-06	4.9E-04	4.9E-04
1599	65	0.175	1.250	830	0.000 ± 0.000	0	0.428	0.0E+00	5.7E-04	5.7E-04

Table 6: Summary of the p_T , I_{as} , $1/\beta$, and mass thresholds, the observed and predicted yields passing these criteria, and the resulting expected (Exp.) and observed (Obs.) cross section limits for modified Drell–Yan models of various charge signals. The signal efficiency and theoretical (Th.) cross section are also listed.

Mass	p_T (GeV)	Requirements			Yields		Signal Eff.	Th.	σ (pb)	
		I_{as}	$1/\beta$	M (GeV)	Predicted	Data			Exp.	Obs.
Modified Drell–Yan $ Q = 1e$ particles with the tracker+TOF analysis										
600	65	0.175	1.250	340	0.002 ± 0.001	0	0.414	1.2E-03	5.9E-04	5.9E-04
800	65	0.175	1.250	460	0.001 ± 0.000	0	0.439	2.6E-04	5.6E-04	5.6E-04
1000	65	0.175	1.250	560	0.000 ± 0.000	0	0.416	7.6E-05	5.9E-04	5.9E-04
1400	65	0.175	1.250	730	0.000 ± 0.000	0	0.328	9.0E-06	7.5E-04	7.5E-04
1800	65	0.175	1.250	890	0.000 ± 0.000	0	0.255	1.0E-06	9.8E-04	9.8E-04
2600	65	0.175	1.250	1040	0.000 ± 0.000	0	0.096	0.0E+00	2.5E-03	2.5E-03
Modified Drell–Yan $ Q = 2e$ particles with the tracker+TOF analysis										
200	65	0.175	1.250	0	2.63 ± 0.53	5	0.202	3.0E-01	1.9E-03	3.3E-03
400	65	0.175	1.250	60	1.45 ± 0.29	2	0.397	2.3E-02	8.2E-04	1.1E-03
600	65	0.175	1.250	150	0.073 ± 0.015	0	0.458	3.5E-03	5.3E-04	5.3E-04
800	65	0.175	1.250	220	0.017 ± 0.003	0	0.462	8.0E-04	5.2E-04	5.2E-04
1400	65	0.175	1.250	310	0.004 ± 0.001	0	0.290	2.7E-05	8.5E-04	8.5E-04
2600	65	0.175	1.250	290	0.005 ± 0.001	0	0.066	0.0E+00	3.7E-03	3.7E-03

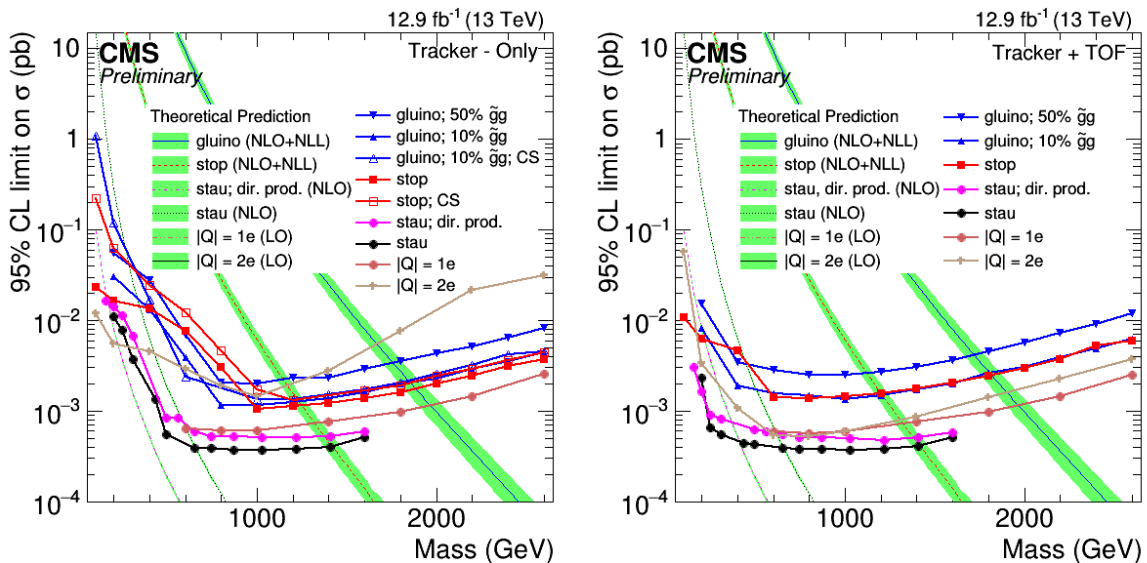


Figure 3: Cross section upper limits at 95% CL on various signal models for the tracker-only analysis (left column) and tracker+TOF analysis (right column) at $\sqrt{s} = 13$ TeV. In the legend, ‘CS’ stands for charged suppressed interaction model.

Table 7: Mass limits obtained using 2016 data for various HSCP candidate models. The expected mass limits are shown in parenthesis. In the model name, 'CS' stands for charged suppressed interaction model.

Model	Analysis	Mass Limits
Gluino $f = 0.1$	tracker-only	$M > 1850(1850)$ GeV
	tracker+TOF	$M > 1810(1810)$ GeV
Gluino $f = 0.1$ CS	tracker-only	$M > 1840(1840)$ GeV
	tracker+TOF	$M > 1760(1760)$ GeV
Gluino $f = 0.5$	tracker-only	$M > 1720(1720)$ GeV
	tracker+TOF	$M > 1800(1800)$ GeV
Stop	tracker-only	$M > 1250(1250)$ GeV
	tracker+TOF	$M > 1200(1200)$ GeV
Stop CS	tracker-only	$M > 1220(1220)$ GeV
GMSB Stau	tracker-only	$M > 660(660)$ GeV
	tracker+TOF	$M > 660(660)$ GeV
Pair Prod. Stau	tracker-only	$M > 170(170)$ GeV
	tracker+TOF	$M > 360(360)$ GeV
DY $Q = 1e$	tracker-only	$M > 720(720)$ GeV
	tracker+TOF	$M > 730(730)$ GeV
DY $Q = 2e$	tracker-only	$M > 670(750)$ GeV
	tracker+TOF	$M > 890(890)$ GeV

- [3] C. W. Bauer et al., "Supermodels for early LHC", *Phys. Lett. B* **690** (2010) 280, doi:10.1016/j.physletb.2010.05.032, arXiv:0909.5213.
- [4] A. Kusenko and M. E. Shaposhnikov, "Supersymmetric Q-balls as dark matter", *Phys. Lett. B* **418** (1998) 46, doi:10.1016/S0370-2693(97)01375-0, arXiv:hep-ph/9709492.
- [5] B. Koch, M. Bleicher, and H. Stoecker, "Black holes at LHC?", *J. Phys. G* **34** (2007) S535, doi:10.1088/0954-3899/34/8/S44, arXiv:hep-ph/0702187.
- [6] J. S. Schwinger, "Magnetic charge and quantum field theory", *Phys. Rev.* **144** (1966) 1087, doi:10.1103/PhysRev.144.1087.
- [7] D. Fargion, M. Khlopov, and C. A. Stephan, "Cold dark matter by heavy double charged leptons?", *Class. Quant. Grav.* **23** (2006) 7305, doi:10.1088/0264-9381/23/24/008, arXiv:astro-ph/0511789.
- [8] Particle Data Group Collaboration, "Review of Particle Physics (RPP)", *Phys. Rev. D* **86** (2012) 010001, doi:10.1103/PhysRevD.86.010001.
- [9] ALEPH Collaboration, "Search for pair production of longlived heavy charged particles in e^+e^- annihilation", *Phys. Lett. B* **405** (1997) 379, doi:10.1016/S0370-2693(97)00715-6, arXiv:hep-ex/9706013.
- [10] DELPHI Collaboration, "Search for heavy stable and longlived particles in e^+e^- collisions at $\sqrt{s} = 189$ GeV", *Phys. Lett. B* **478** (2000) 65, doi:10.1016/S0370-2693(00)00265-3, arXiv:hep-ex/0103038.

[11] L3 Collaboration, “Search for heavy neutral and charged leptons in e^+e^- annihilation at LEP”, *Phys. Lett. B* **517** (2001) 75, doi:10.1016/S0370-2693(01)01005-X, arXiv:hep-ex/0107015.

[12] OPAL Collaboration, “Search for stable and longlived massive charged particles in e^+e^- collisions at $\sqrt{s} = 130$ GeV to 209 GeV”, *Phys. Lett. B* **572** (2003) 8, doi:10.1016/S0370-2693(03)00639-7, arXiv:hep-ex/0305031.

[13] H1 Collaboration, “Measurement of anti-deuteron photoproduction and a search for heavy stable charged particles at HERA”, *Eur. Phys. J. C* **36** (2004) 413, doi:10.1140/epjc/s2004-01894-1, arXiv:hep-ex/0403056.

[14] CDF Collaboration, “Search for long-lived massive charged particles in 1.96 TeV $\bar{p}p$ collisions”, *Phys. Rev. Lett.* **103** (2009) 021802, doi:10.1103/PhysRevLett.103.021802, arXiv:0902.1266.

[15] D0 Collaboration, “Search for long-lived charged massive particles with the D0 detector”, *Phys. Rev. Lett.* **102** (2009) 161802, doi:10.1103/PhysRevLett.102.161802, arXiv:0809.4472.

[16] D0 Collaboration, “A search for charged massive long-lived particles”, *Phys. Rev. Lett.* **108** (2012) 121802, doi:10.1103/PhysRevLett.108.121802, arXiv:1110.3302.

[17] D0 Collaboration, “Search for charged massive long-lived particles at $\sqrt{s} = 1.96$ TeV”, *Phys. Rev. D* **87** (2013), no. 5, 052011, doi:10.1103/PhysRevD.87.052011, arXiv:1211.2466.

[18] ATLAS Collaboration, “Search for heavy long-lived charged particles with the ATLAS detector in pp collisions at $\sqrt{s} = 7$ TeV”, *Phys. Lett. B* **703** (2011) 428, doi:10.1016/j.physletb.2011.08.042, arXiv:1106.4495.

[19] ATLAS Collaboration, “Search for stable hadronising squarks and gluinos with the ATLAS experiment at the LHC”, *Phys. Lett. B* **701** (2011) 1, doi:10.1016/j.physletb.2011.05.010, arXiv:1103.1984.

[20] ATLAS Collaboration, “Search for massive long-lived highly ionising particles with the ATLAS detector at the LHC”, *Phys. Lett. B* **698** (2011) 353, doi:10.1016/j.physletb.2011.03.033, arXiv:1102.0459.

[21] ATLAS Collaboration, “Searches for heavy long-lived sleptons and R-Hadrons with the ATLAS detector in pp collisions at $\sqrt{s} = 7$ TeV”, *Phys. Lett. B* **720** (2013) 277, doi:10.1016/j.physletb.2013.02.015, arXiv:1211.1597.

[22] ATLAS Collaboration, “Search for long-lived, multi-charged particles in pp collisions at $\sqrt{s}=7$ TeV using the ATLAS detector”, *Phys. Lett. B* **722** (2013) 305–323, doi:10.1016/j.physletb.2013.04.036, arXiv:1301.5272.

[23] ATLAS Collaboration, “Searches for heavy long-lived charged particles with the ATLAS detector in proton-proton collisions at $\sqrt{s} = 8$ TeV”, *JHEP* **01** (2015) 068, doi:10.1007/JHEP01(2015)068, arXiv:1411.6795.

[24] ATLAS Collaboration, “Search for heavy long-lived multi-charged particles in pp collisions at $\sqrt{s} = 8$ TeV using the ATLAS detector”, *Eur. Phys. J. C* **75** (2015) 362, doi:10.1140/epjc/s10052-015-3534-2, arXiv:1504.04188.

[25] ATLAS Collaboration, “Search for metastable heavy charged particles with large ionisation energy loss in pp collisions at $\sqrt{s} = 8$ TeV using the ATLAS experiment”, *Eur. Phys. J. C* **75** (2015), no. 9, 407, doi:10.1140/epjc/s10052-015-3609-0, arXiv:1506.05332.

[26] ATLAS Collaboration, “Search for metastable heavy charged particles with large ionization energy loss in pp collisions at $\sqrt{s} = 13$ TeV using the ATLAS experiment”, arXiv:1604.04520.

[27] ATLAS Collaboration, “Search for heavy long-lived charged R -hadrons with the ATLAS detector in 3.2 fb^{-1} of proton–proton collision data at $\sqrt{s} = 13$ TeV”, arXiv:1606.05129.

[28] CMS Collaboration, “Search for heavy stable charged particles in pp collisions at $\sqrt{s} = 7$ TeV”, *JHEP* **03** (2011) 024, doi:10.1007/JHEP03(2011)024, arXiv:1101.1645.

[29] CMS Collaboration, “Search for fractionally charged particles in pp collisions at $\sqrt{s} = 7$ TeV”, *Phys. Rev. Lett.* (2012) arXiv:1210.2311.

[30] CMS Collaboration, “Search for heavy long-lived charged particles in pp collisions at $\sqrt{s} = 7$ TeV”, *Phys. Lett. B* **713** (2012) 408, doi:10.1016/j.physletb.2012.06.023, arXiv:1205.0272.

[31] CMS Collaboration, “Searches for Long-lived Charged Particles in Proton-Proton Collisions at $\sqrt{s} = 13$ TeV”, CMS Physics Analysis Summary CMS-PAS-EXO-15-010, CMS, 2015.

[32] C. F. Berger, J. S. Gainer, J. L. Hewett, and T. G. Rizzo, “Supersymmetry without prejudice”, *JHEP* **02** (2009) 023, doi:10.1088/1126-6708/2009/02/023, arXiv:0812.0980.

[33] M. W. Cahill-Rowley, J. L. Hewett, A. Ismail, and T. G. Rizzo, “More energy, more searches, but the phenomenological MSSM lives on”, *Phys. Rev. D* **88** (2013), no. 3, 035002, doi:10.1103/PhysRevD.88.035002, arXiv:1211.1981.

[34] CMS Collaboration, “Searches for long-lived charged particles in pp collisions at $\sqrt{s} = 7$ and 8 TeV”, *JHEP* **07** (2013) 122, doi:10.1007/JHEP07(2013)122, arXiv:1305.0491.

[35] T. Sjöstrand, S. Mrenna, and P. Z. Skands, “A brief introduction to PYTHIA 8.1”, *Comput. Phys. Commun.* **178** (2008) 852, doi:10.1016/j.cpc.2008.01.036, arXiv:0710.3820.

[36] A. C. Kraan, “Interactions of heavy stable hadronizing particles”, *Eur. Phys. J. C* **37** (2004) 91, doi:10.1140/epjc/s2004-01997-7, arXiv:hep-ex/0404001.

[37] R. Mackeprang and A. Rizzi, “Interactions of coloured heavy stable particles in matter”, *Eur. Phys. J. C* **50** (2007) 353, doi:10.1140/epjc/s10052-007-0252-4, arXiv:hep-ph/0612161.

[38] G. Giudice and R. Rattazzi, “Theories with gauge mediated supersymmetry breaking”, *Phys. Rept.* **322** (1999) 419, doi:10.1016/S0370-1573(99)00042-3, arXiv:hep-ph/9801271.

[39] B. Allanach et al., “The Snowmass points and slopes: Benchmarks for SUSY searches”, *Eur. Phys. J. C* **25** (2002) 113, doi:10.1007/s10052-002-0949-3, arXiv:hep-ph/0202233.

[40] F. E. Paige, S. D. Protopopescu, H. Baer, and X. Tata, “ISAJET 7.69: A Monte Carlo Event Generator for pp , $\bar{p}p$, and e^+e^- Reactions”, (2003). arXiv:hep-ph/0312045.

[41] CMS Collaboration, “The CMS experiment at the CERN LHC”, *JINST* **3** (2008) S08004, doi:10.1088/1748-0221/3/08/S08004.

[42] CMS Collaboration, “Description and performance of track and primary-vertex reconstruction with the CMS tracker”, *JINST* **9** (2014) P10009, doi:10.1088/1748-0221/9/10/P10009, arXiv:1405.6569.

[43] CMS Collaboration, “Performance of CMS muon reconstruction in pp collision events at $\sqrt{s} = 7$ TeV”, *JINST* **7** (2012) P10002, doi:10.1088/1748-0221/7/10/P10002, arXiv:1206.4071.

[44] CMS Collaboration, “Jet performance in pp collisions at $\sqrt{s}=7$ TeV”, CMS Physics Analysis Summary CMS-PAS-JME-10-003, CMS, 2010.

[45] CMS Collaboration, “Particle-flow event reconstruction in CMS and performance for jets, taus, and E_T^{miss} ”, CMS Physics Analysis Summary CMS-PAS-PFT-09-001, CERN, 2009.

[46] CMS Collaboration, “Measurement of tracking efficiency”, CMS Physics Analysis Summary CMS-PAS-TRK-10-002, CMS, 2010.

[47] T. Junk, “Confidence level computation for combining searches with small statistics”, *Nucl. Instrum. Meth. A* **434** (1999) 435, doi:10.1016/S0168-9002(99)00498-2, arXiv:hep-ex/9902006.

[48] A. L. Read, “Presentation of search results: the CL_s technique”, *J. Phys. G* **28** (2002) 2693, doi:10.1088/0954-3899/28/10/313.

[49] G. Cowan, K. Cranmer, E. Gross, and O. Vitells, “Asymptotic formulae for likelihood-based tests of new physics”, *Eur. Phys. J. C* **71** (2011) 1554, doi:10.1140/epjc/s10052-011-1554-0, arXiv:1007.1727.

[50] W. T. Eadie et al., “Statistical methods in experimental physics”. North Holland, Amsterdam, 1971.

[51] F. James, “Statistical methods in experimental physics”. World Scientific, Singapore, 2006.

[52] A. Kulesza and L. Motyka, “Threshold resummation for squark-antisquark and gluino-pair production at the LHC”, *Phys. Rev. Lett.* **102** (2009) 111802, doi:10.1103/PhysRevLett.102.111802, arXiv:0807.2405.

[53] A. Kulesza and L. Motyka, “Soft gluon resummation for the production of gluino-gluino and squark-antisquark pairs at the LHC”, *Phys. Rev. D* **80** (2009) 095004, doi:10.1103/PhysRevD.80.095004, arXiv:0905.4749.

[54] W. Beenakker et al., “Soft-gluon resummation for squark and gluino hadroproduction”, *JHEP* **12** (2009) 041, doi:10.1088/1126-6708/2009/12/041, arXiv:0909.4418.

- [55] W. Beenakker et al., “Supersymmetric top and bottom squark production at hadron colliders”, *JHEP* **08** (2010) 098, doi:10.1007/JHEP08(2010)098, arXiv:1006.4771.
- [56] W. Beenakker, R. Hopker, and M. Spira, “PROSPINO: A program for the PROduction of Supersymmetric Particles In Next-to-leading Order QCD”, arXiv:hep-ph/9611232.
- [57] P. M. Nadolsky et al., “Implications of CTEQ global analysis for collider observables”, *Phys. Rev. D* **78** (2008) 013004, doi:10.1103/PhysRevD.78.013004, arXiv:0802.0007.